ELSEVIER

Earth and Planetary Science Letters 120 (1993) 409–430

EPSL

The Vendian record of Sr and C isotopic variations in seawater: Implications for tectonics and paleoclimate

Alan J. Kaufman [a], Stein B. Jacobsen [a], Andrew H. Knoll [b]

[a] *Harvard Center for Isotope Geochemistry, Department of Earth and Planetary Sciences Harvard University, 20 Oxford Street, Cambridge, MA 02138, USA*

[b] *Department of Organismic and Evolutionary Biology, Harvard University, 20 Oxford Street, Cambridge, MA 02138, USA*

(Received May 19, 1993; revised and accepted September 24, 1993)

Abstract

New Sr and C isotopic data, both obtained on the same samples of marine carbonates, provide a relatively detailed record of isotopic variation in seawater through the latest Proterozoic and allow, for the first time, direct correlation of these isotopic changes in the Vendian (~ 540–610 Ma). The strong isotope variations determined in this study record significant environmental and tectonic changes. Together with a fairly poorly constrained Nd isotopic record, the Sr and C isotopic records can be used to constrain rates of erosion, hydrothermal alteration and organic C burial. Further, comparison of these records with those of the Cenozoic permit investigation of the general relationship between global tectonics and continental glaciation. In particular, results of this study show a very large change in the $^{87}Sr/^{86}Sr$ of marine carbonates from low pre-Vendian (> 610 Ma) values (~ 0.7066) to high Middle Cambrian values (~ 0.7090). This change is greater in magnitude than the significant increase in seawater $^{87}Sr/^{86}Sr$ through the Cenozoic. Both changes are attributed to high erosion rates associated with continent–continent collisions (Pan-African and Himalayan–Tibetan). In the latest Proterozoic these high erosion rates, probably coupled with high organic productivity and anoxic bottom-water conditions, contributed to a significant increase in the burial rate of organic C. Ice ages mark both the Neoproterozoic and Cenozoic, but different stratigraphic relationships between the Sr isotopic increase and continental glaciation indicate that uplift-driven models proposed to explain Cenozoic climatic change cannot account for the latest Proterozoic ice ages.

1. Introduction

During the past 100 Ma, the $^{87}Sr/^{86}Sr$ of sea water has increased almost monotonically, from about 0.7076 to 0.7092 [1]. Rates of increase were particularly high between 40 and 15 Ma ago. Secular variation in $^{87}Sr/^{86}Sr$ of sea water results primarily from variation in continental erosion, the isotopic composition of eroding continental rocks and the hydrothermal flux from mid-ocean ridges. The Cretaceous/Cenozoic pattern has been attributed to increased erosional flux from the continents, associated, at least in part, with uplift of the Himalayas and Tibetan Plateau, and to increasing erosion of extremely radiogenic crust [2–5].

Strontium isotopic variation for the Vendian (~ 540–610 Ma [6]) and Cambrian periods resembles that for the last 100 Ma of the Phanerozoic in that $^{87}Sr/^{86}Sr$ increased from ~ 0.707 prior to

[CL]

Elsevier Science Publishers B.V.
SSDI 0012-821X(93)E0181-I

the Varanger glacial episode (ca. 590–610 Ma) to ~0.709 by Middle Cambrian times [7]. A closer comparison of the two intervals requires that the older isotopic record be reconstructed in more detail than has hitherto been available. In this paper, we present improved data on the Sr isotopic record of sea water through most of the Vendian, based principally on carbonates from the Polarisbreen Group in Svalbard and equivalents in East Greenland, the Witvlei and Nama groups in Namibia and South Africa, and the upper Windermere Supergroup in the Northwest Territories of Canada.

Large variations in the isotopic composition of C, S, Nd and Sr are recorded in Neoproterozoic (540–1000 Ma) successions and these appear to be much larger than those preserved in Cenozoic successions. Simple first-order models have been developed to interpret these records [2,7,8]. These models suggest that the Vendian was a time of both extremely high erosion rates and of significant organic C burial—perhaps greater than any other period of Earth history. The Vendian Sr isotopic record is consistent with, and may require that, Pan-African orogenesis produced Himalayan-scale mountains during the latest Proterozoic and Cambrian [7].

Recognition of major orogenic uplift at this time is important in another context. It has been suggested that late Cenozoic uplift altered patterns of atmospheric circulation and increased rates of chemical weathering, resulting in decreased atmospheric pCO_2 and continental glaciation [4,9]. In so far as major ice ages also characterize the Neoproterozoic, the Sr and Nd isotopic curves for this period permit us to evaluate the generality of the proposed relationship between tectonics and climate.

2. Geology

2.1 Polarisbreen Group and equivalents, Svalbard and East Greenland

The Polarisbreen Group and its equivalents in Svalbard and East Greenland have recently been the focus of several detailed studies [10–12]. The group comprises a thick succession of shallow marine and lacustrine carbonates and siliciclastics which alternate with glacial deposits. In Svalbard, the group is divided into the Elbobreen, Wilsonbreen and Dracoisen formations. Two tillite horizons occur in this succession, one each in the Elbobreen and Wilsonbreen Formations; both horizons are attributed to the Varanger Ice Age. The Polarisbreen Group sits disconformably above the late Riphean Backlundtoppen Formation of the Akademikerbreen Group and below the Early Cambrian Blårevbreen Sandstone. The hiatus between the Polarisbreen and Akademikerbreen groups has been estimated at 50–70 Ma [8] but could be significantly smaller.

Deposition of the Polarisbreen Group occurred under predominantly marine conditions; however, a number of horizons, including intervals within both the Wilsonbreen and Dracoisen formations, have been interpreted as lacustrine [10].

2.2 Nama and Witvlei Groups, Namibia and South Africa

The stratigraphy, sedimentology, depositional and diagenetic environments, paleontology and age of the Vendian Nama and Witvlei groups in Namibia have been the focus of several recent studies [13,14] and more detailed information can be found there. In brief, the Witvlei Group and Kuibis and Schwarzrand subgroups of the Nama Group represent a thick succession of mixed carbonate and siliciclastic lithologies deposited on a shallow marine platform. The uppermost unit of the Nama Group, the Fish River Subgroup, is a thick redbed succession that disconformably overlies the marine rocks of the lower two subgroups. A significant unconformity is inferred to separate the lower Court (lacustrine) and upper Buschmannsklippe (marine) formations of the Witvlei Group [15]. Germs [13] indicated that an unconformity also separates the Witvlei and Nama groups, but recent field investigations in the Gobabis area suggest that this boundary is, at least locally, transitional [W. Hegenberger, pers. commun., 1990]. In a detailed C isotopic study, Kaufman et al. [16] indicate that the hiatus between

the Court and Buschmannsklippe formations may be coeval with a period of continental glaciation, possibly represented by the Numees tillite of the Gariep Group in Namibia. Hoffmann [15], however, considers that the Gariep Group is older than the Witvlei Group.

Correlation of the flat-lying and relatively untectonized Nama and Witvlei groups in Namibia with apparently coeval sediments in South Africa is complicated by a lack of continuous outcrop, as well as poor exposure and extreme tectonic folding and faulting in the northern Cape Province of South Africa [14]. Earlier lithostratigraphic correlations by Kröner [17] suggest that carbonates in the Grootreit Formation of the Vanrhynsdorp Group near Vanrhynsdorp, South Africa, are equivalent to carbonates in the Kuibis Subgroup. This correlation formed the stratigraphic basis for the interpretation of carbonate samples collected around Vanrhynsdorp and featured in two earlier isotopic studies [18,19]. Subsequent field work in Namibia and South Africa has resulted in a reinterpretation of this correlation. Germs and Gresse [14] note that virtually all of the stratigraphic units of the Vanrhynsdorp Group resemble strata of the Schwarzrand Subgroup, which overlies the Kuibis Subgroup in Namibia. In particular, the Grootriet Formation limestones, which contain both oolites and catagraphs, are lithologically similar to those in the Huns Member of the Schwarzrand Subgroup; Germs and Gresse [14] thus suggest that they are probably equivalent units.

2.3 Windermere Supergroup, Arctic Canada

The upper succession of the Windermere Supergroup contains three siliciclastic to carbonate "Grand Cycles" which include, in ascending order, the Twitya-Keele, Sheepbed-Gametrail and Blueflower-Risky formations [20–22]. In the Mackenzie Mountains, shallow-water carbonates of the late Riphean to earliest Vendian Keele Formation are disconformably overlain by the Ice Brook Formation, a recently discovered diamictite attributed to the Varanger glacial episode [21]. The Keele and Ice Brook formations are overlain by a thin unit known as the "Tepee dolomite" [21], which is similar to numerous other "cap" dolomites that occur above glacial deposits of this age worldwide.

Above the "Tepee dolomite", the Sheepbed Formation consists of siliciclastics and minor fine-grained limestones that pass upward into massive dolostones of the Gametrail Formation [20,23]. Gametrail carbonates contain gashes of baroque dolomite suggestive of significant hydrothermal alteration. The uppermost "Grand Cycle" begins with siliciclastic mudstone and turbiditic sandstone punctuated by thin horizons of ribbon-bedded limestone (the Blueflower Formation), followed by dolomites and limestones of the Risky Formation. At the top of the Risky Formation is a karstic disconformity that marks the top of the Windermere Supergroup [22]. The Neoproterozoic–Cambrian transition is thought to occur within the overlying Ingta Formation, which consists predominantly of sandstones and siltstones of shallow-shelf origin.

3. Age constraints

As in the Phanerozoic Eon, latest Neoproterozoic rocks can be correlated by means of fossils and other chronostratigraphic indicators. Absolute age estimates come from a limited number of radiometric calibration points. In this paper we use the Vendian time scale and correlation scheme proposed by Knoll and Walter [6] and references therein. The base of the Vendian is placed at 610 Ma, the Ediacaran faunal interval spans the time from 580 to 560 Ma, and the Proterozoic–Cambrian boundary is placed at 540 Ma. Thus, the age of each succession can be broadly constrained by paleontological and chronostratigraphic evidence, as well as the position of Varanger diamictites. Given these constraints, ages are placed at several points within each succession.

The age of the Polarisbreen Group is constrained at its base by the presence of Varanger age glacial deposits and at its top by the occurrence of Early Cambrian fossils in rocks immediately above the Dracoisen Formation. However, the absence of Ediacaran trace and body fossils,

latest Vendian acritarchs, and the distinctive, middle Vendian, C-isotope positive excursion suggests that the upper Polarisbreen Group was deposited before ~580 Ma. Using the combined litho- and bio-stratigraphic information and the empirical subsidence model of Sleep [24]:

$$T = T_0 + \tau_e \ln\left[1 - \frac{D}{A_0 \tau_e}\right] \quad (1)$$

where τ_e = the erosion rate time constant (assumed to be 50 Ma^{-1}); A_0 = the initial sedimentation rate; D = the stratigraphic height; and T_0 = the age of the oldest sediments at the base of the section; ages can be assigned to each sample within the group. Assuming ages of 585 and 610 Ma for the top and bottom of this succession, then, with $T_0 = 610$ Ma and a total thickness of 1170 m, we obtain an initial sedimentation rate (A_0) of 59.47 m Ma^{-1}. This yields ages of 598 Ma and 606 Ma at the top of the upper and lower glacial horizons, respectively. An age of 601 Ma was calculated for the boundary between the Elbobreen and Wilsonbreen Formations. The age of 598 Ma for the end of the Varanger Ice Age in the Polarisbreen succession will also be used as a constraint for the Nama-Witvlei and Windermere successions. By this method relative ages are well constrained: absolute age estimates are less certain, however, due to uncertainty in the chronometric ages of tie points, as well as the simplification of using eq. (1). Nonetheless, calculated ages are useful for correlating samples from different successions.

The age of the Nama Group, from the base of the Kliphoek Member in the Kuibis Subgroup to the top of the Huns Member in the Schwarzrand Subgroup, is constrained between 560 and 580 Ma by the presence of Ediacaran metazoans. The Feldschuhorn and Spitzkop formations record an additional several million years, estimated here by extrapolation of the subsidence curve. The age of the Nomtsas Formation, which lies unconformably above the Spitzkop Member, remains uncertain, but the presence of the trace fossils *Phycodes pedum* and *Diplichnites* suggests an Early Cambrian age. For this study, a 70 m thick section of the Nomtsas Formation is assumed to span the time from 535–540 Ma. For this short time interval we estimate ages by linear interpolation. Available paleomagnetic data and radiometric dates roughly corroborate ages suggested by paleontological data for the Nama Group. The base of the Buschmannsklippe Formation of the underlying Witvlei Group sits above an unconformity interpreted as being of Varanger age [15]. Our Vendian section from this area has a total thickness of 815 m. The lower part includes the Ediacaran, in the range 235–695 m, and is thus estimated to cover the time span 592–552 Ma. Using $D = 695$ m at 560 Ma and $D = 235$ m at 580 Ma we obtain $A_0 = 48.50$ m Ma^{-1}. Extrapolation of the subsidence model described above to sediments below the Ediacaran interval in the Nama Group indicates an age of $T_0 = 592$ Ma for the base of the succession and 552 Ma for the top (i.e., 815 m).

The upper Windermere Supergroup, from the base of the "Tepee dolomite" to the middle of the Ingta Formation, is approximately 2140 m thick and is assumed to span the entire period from the top of the Varanger glacials (extrapolated from the Polarisbreen Group to be 598 Ma) to the Precambrian–Cambrian boundary at 540 Ma. Ediacaran assemblages have been described from sediments in the middle of the Sheepbed Formation, at approximately 450 m, to the top of the Blueflower Formation at 1770 m. The trace fossil *Phycodes pedum* and elements of the *P. pedum* Zone sensu Narbonne [25] occur within the Ingta Formation and can be used to recognize the base of the Cambrian in the Mackenzie Mountains. Using $T_0 = 598$ Ma and $D = 2140$ m at 540 Ma we obtain $A_0 = 62.34$ m Ma^{-1}.

Fig. 1 shows a comparison of the ages of the three successions. Constraints on ages of all samples, as determined by the subsidence model calculations, along with the distribution of limestone and dolostone samples used in this study, are summarized in Fig. 2. The similar A_0 values obtained for each of the successions suggests that overall sedimentation rates in each of the Vendian basins were roughly similar. However, we recognize that within each sequence sedimentation rates may have varied significantly—particularly during periods of continental glaciation.

4. Samples and methods

4.1 Samples

Limestones and dolostones from southern Africa used in this study were collected from outcrop exposures by AJK in 1990 with the generous assistance of Pieter Gresse (South African Geological Survey, Cape Town) and Wulf Hegenberger (Namibian Geological Survey, Windhoek), or were samples used previously in the study by Kaufman et al. [16]. Additional carbonate samples from the Polarisbreen Group and its equivalents in Svalbard and East Greenland were provided by Ian Fairchild (University of Birmingham) and Keene Swett (University of Iowa), or were samples described in Knoll et al. [11] or Derry et al. [8,26]. All samples analyzed here feature facies relationships, lateral dimensions and thicknesses, and (in some cases) fossils indicative of a marine origin.

4.2 Methods

Whole-rock powders were prepared from field samples using techniques described in Wedeking et al. [27]. In addition, polished thin and thick sections were prepared from a selected suite of samples for petrographic and cathodoluminescence (CL) examination, respectively. Where possible, non-luminescent (NLM) or moderately luminescent microspar (MLM) was isolated (5–10 mg) by microdrilling techniques from thick sections (cf. Kaufman et al., [16]). For the determination of Mn, Sr, Mg and Ca concentrations in carbonate, aliquots of whole-rock and microdrilled powders were weighed and leached in ultra clean, weak (0.5 *M*) acetic acid to avoid the dissolution of clastic components noted to occur with the use of even dilute solution of HCl. After leaching, solutions were decanted and diluted in 2% HNO_3; residues were dried and weighed to determine the percentage dissolution. Elemental analyses were performed on a VG PQ2 + plasma source mass spectrometer. Gravimetrically determined standards were analyzed in order to develop response calibration curves and a 100 ppb ^{115}In spike was added for normalization. Accuracy of elemental abundances determined by this technique are better than ±5% compared to isotope dilution techniques.

Carbon dioxide was evolved from powders of limestone for determination of $\delta^{13}C$ and $\delta^{18}O$ by reaction with concentrated H_3PO_4 ($\rho > 1.89$ g/ml) at 90°C in the auto-sample magazine of a VG PRISM gas isotope ratio mass spectrometer. Since a much longer reaction time is necessary for the quantitative digestion of dolostone powders, CO_2 in these samples was exsolved using off-line techniques under identical conditions and was subsequently isolated by cryogenic distillation. Fractionation factors used for the calculation of ^{18}O abundances of calcites and dolomites based on analyses of CO_2 prepared at 90°C were 1.00798 and 1.00895, respectively. Accuracy of these isotopic techniques, as determined by multiple de-

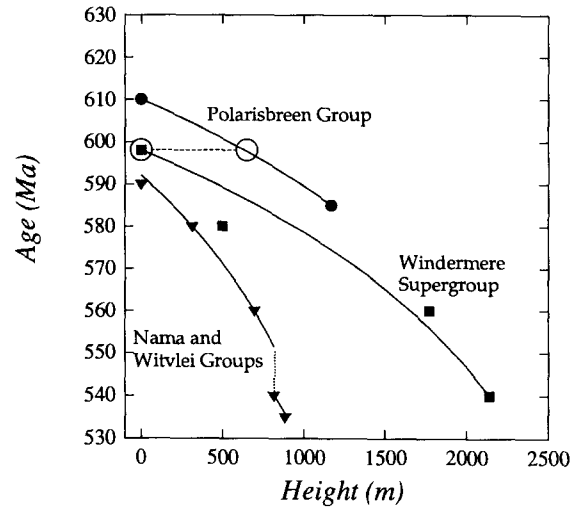

Fig. 1. Comparison of stratigraphic height against age relationships calculated by an empirical subsidence model (see text) determined for Vendian-aged basins used in this study. Tie points connected by a dashed line relate to comparable stratigraphic horizons within the Polarisbreen and upper Windermere successions related to the position of the termination of the Varanger glaciation. The circles represent the calculated age of the correlation point at the top of the glacial horizon in the Upper Windermere Supergroup at 598 Ma. The break in the subsidence curve for the Nama/Witvlei groups represents an inferred hiatus near the top of the sequence. Ages of individual samples in this study were calculated using these relationships.

terminations ($n > 25$) of standard materials, is ± 0.1 for $\delta^{13}C$ and ± 0.3 for $\delta^{18}O$.

A third aliquot of microsample or whole-rock powder was leached in 0.5 *M* acetic acid for determination of Rb and Sr concentrations, $^{87}Rb/^{86}$ Sr and $^{87}Sr/^{86}Sr$. After centrifugation, the supernate was decanted, dried and redissolved in 1.5 *M* HCl. A 1% aliquot of the solution was removed and spiked with isotopic tracers for Rb and Sr. Concentrations of these elements were determined by isotope dilution techniques on a Finnigan THQ thermal ionization mass spectrometer. Strontium was separated from the remaining solution by standard ion exchange techniques and isotopic compositions determined on a Finnigan MAT 262 thermal ionization mass spectrometer with static multi-collection. Interference from ^{87}Rb was monitored by measuring ^{85}Rb with an ion counter. Multiple NBS 987 standards analyzed during the course of this work yield an average value of 0.710241 ± 8 (uncertainty given as 2σ of the mean) and replicate analyses of modern Pacific seawater resulted in an average value of 0.709174 ± 5.

5. Results

5.1 Petrography and cathodoluminescence

After an initial period of investigation on the elemental and Sr isotopic compositions of fine-grained whole-rock (WR) carbonate samples, detailed studies of microsample carbonate were undertaken on a selected suite of representative rocks. Petrographic and cathodoluminescence examination on this suite of samples show that individual samples commonly exhibit wide variations in texture. Organic C abundance also varies considerably within and among samples. Nonluminescent portions of the samples have been recognized as representing the least-altered ma-

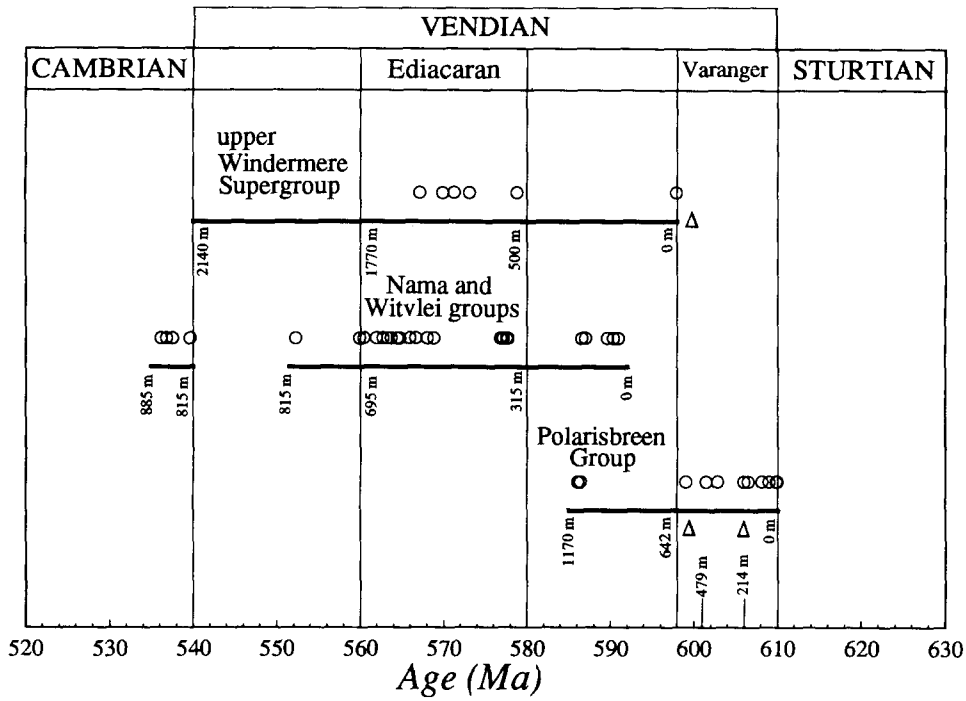

Fig. 2. Stratigraphy, ages and sample distribution. Correlation of successions and distribution of samples plotted against calculated ages. The position of the Ediacaran and Varanger intervals are shown, as well as the calculated position of glacial horizons; these horizons are represented by triangles within the Polarisbreen Group and at the base of the upper Windermere Supergroup.

terial [16]. Therefore, where possible, microsamples were isolated from zones composed of non-luminescent microspar (NLM) or dolomicrospar for subsequent elemental and isotopic analyses. Most dolostone samples in this study were texturally homogeneous and had higher luminescence than limestone samples. Although early dolomitization, in many examples, preserves the primary textural features of these carbonates, it is unlikely that this process preserves primary elemental and isotopic compositions of minor and trace elements.

5.2 Elemental and isotopic compositions

To illustrate the elemental and Sr isotopic heterogeneity within a single sample, Mn/Sr and $^{87}Sr/^{86}Sr$ of variably luminescent microsamples and of WR carbonate are presented in Fig. 3 from sample SH 12 of the Huns Member of the Nama Group (cf. fig. 5 in [16]). Microsamples were isolated from two zones of the least recrystallized/altered portion of the sample (non-luminescent microspar: NLM1 and NLM2), moderately altered/recrystallized portions (mod-

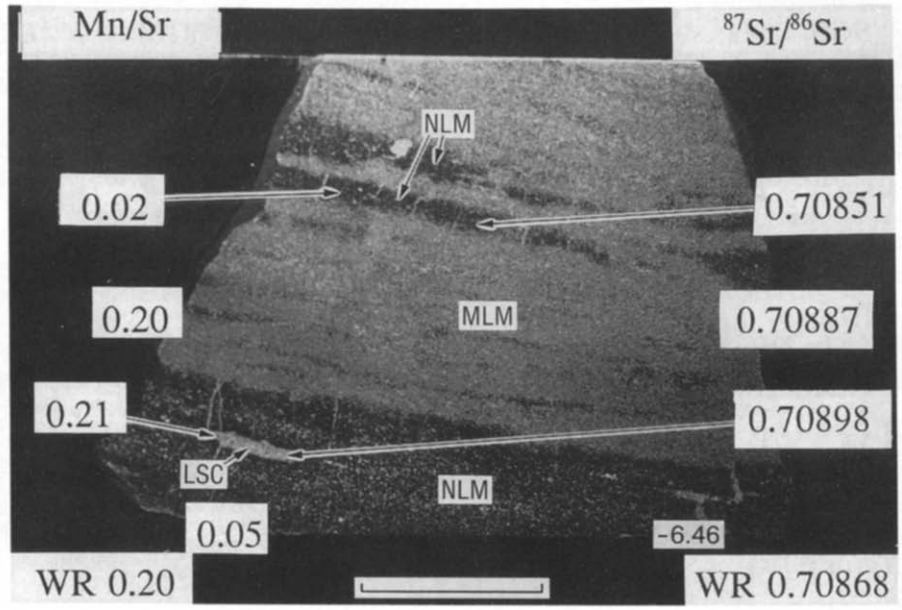

sample	$\delta^{13}C$	$\delta^{18}O$	Mg/Ca	Sr (ppm)	$^{87}Rb/^{86}Sr$
	(‰, PDB)				
WR	0.8	-14.1	0.002	1793	0.00129
NLM1	1.3	-6.5	0.004	3336	0.000358
NLM2	1.4	-6.8	0.006	3088	0.000573
MLM	0.8	-14.8	0.005	1305	0.00132
LSC	0.6	-15.0	0.005	882	0.00227

Fig. 3. Photograph of a highly polished section of sample SH 12 under cathodoluminescence. Mn/Sr and $^{87}Sr/^{86}Sr$ of non-luminescent microspar (NLM), moderately luminescent microspar (MLM), luminescent sparry calcite (LSC) and whole-rock (WR) carbonate are shown. Scale bar = 1 cm (cf. [16]). Additional data for each of the microsamples and whole-rock carbonates are tabulated below the photograph.

Table 1
Isotopic and elemental compositions of Vendian carbonates

number	sample[1]	height[2] (m)	age[3] (Ma)	$\delta^{13}C$ ‰, PDB	$\delta^{18}O$ ‰, PDB	Sr[4] (ppm)	Mn/Sr[5]	Mg/Ca	Ca/Sr	$^{87}Rb/^{86}Sr$[4]	$^{87}Sr/^{86}Sr_{meas}$[5]	$^{87}Sr/^{86}Sr_{init}$[6]
Polarisbreen Group and equivalents, Svalbard and East Greenland												
61892	NLM	1130	586.1	-0.2	-6.0	37	1.68	0.138	--	0.0494	0.709683	0.709271
Y-SC	NLM	1130	586.1	-0.8	-9.5	184	0.59	0.512	--	0.00830	0.708379	0.708310
Y-GR	MLM	1120	586.4	-1.2	-7.4	63	1.14	0.588	--	0.0297	0.709528	0.709279
P 7380	MLM	587	599.0	4.1	-2.1	81	2.42	0.552	--	0.00267	0.707939	0.707916
F 6948	NLM	467	601.5	4.1	-2.6	194	2.09	0.552	--	0.0277	0.708053	0.707816
61928	NLM	398	602.8	-0.3	-4.7	420	1.32	0.035	--	0.000954	0.706839	0.706831
N Ni 10+	NLM	230	606.0	3.2	-10.4	530	0.82	0.010	--	0.000720	0.707006	0.707000
P126	WR	202	606.5	4.4	-6.5	125	0.15	0.563	188	0.0157	0.708686	0.708550
P 123	NLM	108	608.2	2.8	-2.6	52	2.92	0.599	--	0.00117	0.707377	0.707367
M 45	WR	61	609.0	6.1	-5.2	2508	0.03	0.004	168	0.000231	0.706644	0.706642
M 44	WR	59	609.0	3.6	-5.9	1049	0.52	0.042	190	0.000231	0.707414	0.707412
M 38	NLM	10	609.8	5.3	-4.5	3705	0.13	0.015	--	0.000666	0.706612	0.706606
M 37	NLM	3	609.9	1.1	-5.6	1594	0.66	0.013	--	0.00121	0.706754	0.706743
M 39	NLM	1	610.0	4.4	-5.6	430	0.55	0.005	--	0.00405	0.707134	0.707099
Nama and Witvlei groups, Namibia and South Africa												
SN 102	NLM	870	536.1	1.7	-13.4	1512	0.75	0.009	--	0.00195	0.708700	0.708685
SN 103	WR	860	536.8	0.8	-13.0	1519	1.42	0.009	218	0.000200	0.708919	0.708917
GG 76	NLM	850	537.5	-1.2	-4.9	123	0.99	0.472	--	0.0199	0.709420	0.709269
GG 2B	NLM	850	537.5	1.7	-10.2	563	0.28	0.599	--	0.0109	0.709617	0.709534
GG 3	WR	850	537.5	1.6	-9.7	391	0.78	0.338	232	0.00610	0.709093	0.709047
SN 75	WR	820	539.6	1.8	-9.8	349	0.24	0.240	281	0.00216	0.709397	0.709381
SS 17	WR	805	552.2	1.7	-8.1	1591	0.04	0.002	84	0.000170	0.708514	0.708512
SH 12	NLM1	695	559.9	1.3	-6.5	3336	0.05	0.004	--	0.000358	0.708457	0.708454
NG 91	WR	687	560.4	1.4	-8.7	1886	0.22	0.004	218	0.000051	0.708585	0.708585
SH 43	WR	663	561.9	1.2	-9.5	1520	0.02	0.002	--	0.000087	0.708532	0.708531
NG 90	WR	651	562.7	2.4	-7.4	1493	0.08	0.006	255	0.000120	0.708566	0.708565
SH 54	WR	642	563.2	1.5	-8.7	708	0.03	0.003	161	0.000453	0.708581	0.708581
NG 87	WR	635	563.7	2.0	-10.3	2093	0.06	0.001	164	0.000028	0.708566	0.708566
NG 86	NLM	623	564.4	2.2	-12.9	637	0.20	0.006	--	0.000499	0.708849	0.708845
SH 49	WR	617	564.7	1.6	-7.5	1979	0.03	0.005	156	0.000077	0.708494	0.708493
NG 85	NLM	596	565.9	-0.8	-8.8	1029	0.07	0.001	--	0.000215	0.708578	0.708576
NG 84	WR	584	566.6	-0.5	-9.5	729	0.25	0.001	2320	0.000328	0.708707	0.708704
NG 83	WR	560	568.0	0.1	-8.9	1856	0.10	0.001	503	0.000119	0.708518	0.708517
NG 81	WR	545	568.8	0.1	-7.8	598	0.93	0.001	869	0.000452	0.708682	0.708678
NG/N 2	WR	385	576.8	0.2	-9.5	457	0.64	0.011	444	0.00566	0.708490	0.708444
KS 145	NLM	383	576.9	3.0	-6.8	486	0.98	0.010	--	0.000797	0.708543	0.708537
KMO 115	NLM	380	577.0	6.6	-8.9	695	0.09	0.013	--	0.0148	0.709279	0.709158
KMO 116	NLM	379	577.1	5.3	-11.7	313	0.30	0.011	--	0.134	0.709531	0.708442
KO 140	NLM	370	577.5	2.8	-8.6	623	0.75	0.031	59	0.000382	0.708842	0.708840
KO 137	NLM	365	577.7	2.1	-8.3	3596	0.01	0.005	--	0.000052	0.708398	0.708397

Table 1 (*continued*)

WG 11	WR	153	586.5	-4.3	-6.3	280	1.56	0.348	--	0.00240	0.708629	0.708609
WG 9	NLM	139	587.0	-4.4	-10.2	1176	0.56	0.011	--	0.00130	0.708176	0.708165
WG 20	WR	70	589.6	-5.5	-13.3	610	2.36	0.007	267	0.00334	0.708651	0.708623
WG 8	WR	49	590.3	-5.0	-10.8	745	0.67	0.009	374	0.00153	0.708140	0.708127
WG 7	NLM	32	590.9	-5.3	-13.5	245	0.92	0.007	--	0.0152	0.709800	0.709674
upper Windermere Supergroup, Northwest Territories, Canada												
N91-23K	NLM	1435	567.1	2.1	-7.6	1467	0.04	0.006	322	0.000635	0.708616	0.708611
N91-23H	NLM	1340	569.9	1.0	-4.9	1249	0.06	0.017	231	0.00103	0.708607	0.708599
N91-23F	NLM	1290	571.3	0.5	-7.7	1410	0.06	0.008	233	0.00124	0.708416	0.708406
N91-23A	NLM	1222	573.1	2.2	-7.5	791	0.08	0.006	140	0.00161	0.708551	0.708538
N91-21-25	NLM	995	578.8	5.9	-11.0	1306	0.64	0.015	351	0.00476	0.708892	0.708859
N89-128A	NLM	8	597.9	-4.6	-10.4	1374	0.07	0.007	707	0.000418	0.707226	0.707223
N92-14H	NLM	-225		8.2	-9.8	669	0.17	0.009	636	0.00152	0.707342	0.707342
N89-132	NLM	-398		8.2	-7.3	904	0.10	0.001	160	0.00145	0.707124	0.707124

[1] WR = whole-rock, NLM = non-luminescent microspar, MLM = moderately luminescent microspar.

[2] Approximate measurements above base of (1) Elbobreen Formation, Polarisbreen Group, Svalbard; (2) Buschmannsklippe Formation, Witvlei Group, Namibia; and (3) "Tepee dolomite", upper Windermere Supergroup, Northwest Territories, Canada.

[3] Ages of individual samples calculated from a basinal subsidence model (see text for discussion of individual units).

[4] Concentrations and ratios determined by isotope dilution techniques.

[5] Corrected for mass fractionation using $^{86}Sr/^{88}Sr = 0.1194$.

[6] Value corrected using calculated individual ages and a half-life of ^{87}Rb of 1.42×10^{-11} y.

erately luminescent microspar: MLM), and a very late, highly recrystallized, luminescent sparry calcite (LSC). In thin section, carbonate textures in NLM zones are slightly finer grained than those in MLM zones. In addition, NLM has a relatively greater abundance of organic C relative to MLM. There is no variation in the abundance of iron-rich clays or hematite between the two zones but, as shown, Mn/Sr and $^{87}Sr/^{86}Sr$ vary significantly. The $\delta^{13}C$, $\delta^{18}O$, Mg/Ca, $^{87}Rb/^{86}Sr$ and Sr concentrations on these microsamples are tabulated below the photograph in Fig. 3.

The two NLM zones have very similar Sr concentrations, Mn/Sr, $^{87}Rb/^{86}Sr$ and $^{87}Sr/^{86}Sr$. The MLM, LSC and WR samples all have lower Sr concentrations and higher Mn/Sr, $^{87}Rb/^{86}Sr$ and $^{87}Sr/^{86}$ Sr relative to the NLM zones. Higher Mn/Sr has been attributed to the addition of Mn and/or the removal of Sr during meteoric diagenesis [19]. This example is consistent with previous studies [7,8,19] in that NLM zones with the lowest Mn/Sr, $^{87}Rb/^{86}Sr$ and $^{87}Sr/^{86}Sr$, as well as the highest $\delta^{13}C$ and $\delta^{18}O$ values, appear to represent the least-altered carbonate phase. The difference of 0.0002 in $^{87}Sr/^{86}Sr$ values between NLM and WR carbonate, although small in this example, shows that Sr isotopic compositions of contemporaneous seawater may not always be represented by whole-rock analyses.

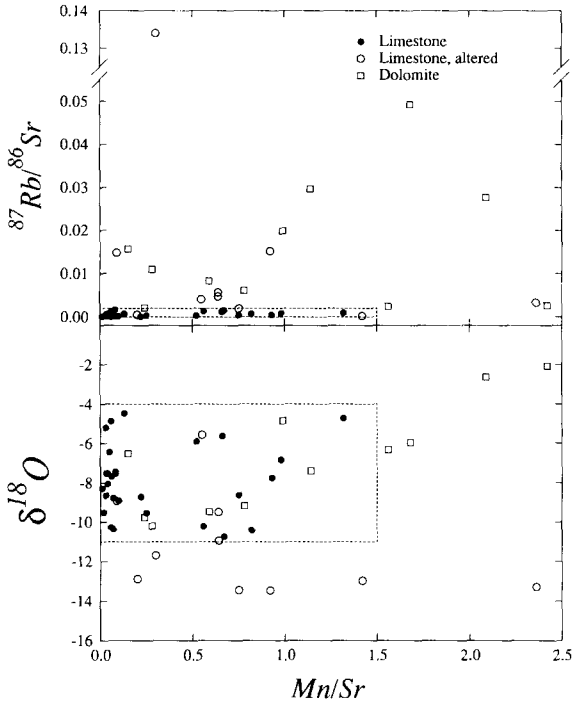

Fig. 4. Plot of $^{87}Rb/^{86}Sr$ and $\delta^{18}O$ against Mn/Sr for all limestone and dolostone samples used in this study. Dashed boxes represent our best estimate for the field of least-altered samples. These include samples with Mn/Sr < 1.5, $\delta^{18}O < -11$ and $^{87}Rb/^{86}Sr < 0.001$.

Results of elemental and isotopic analyses on all whole-rock and microdrilled carbonates are presented in Table 1. This suite of samples includes those that passed an initial screening of ~ 300 samples. We included for isotopic analysis only limestones and dolostones satisfying the following criteria: (1) low abundances of siliciclastic material; (2) relatively fine-grained texture; (3) low to moderate luminescence; and (4) Mn/Sr < 3. We have highest confidence that limestones with Mn/Sr < 1.5, $^{87}Rb/^{86}Sr < 0.001$, and $\delta^{18}O > -11$ most probably record near-primary C and Sr isotope compositions (Fig. 4). Although some dolostones in this study fall within the Mn/Sr and $\delta^{18}O$ boundaries set for unaltered samples (Fig. 4b), elevated $^{87}Rb/^{86}Sr$ and low Sr concentrations (Table 1) suggest that the Sr isotopic compositions of these are altered. NLM carbonates with high $\delta^{13}C$ and $\delta^{18}O$ values and low Mn/Sr, $^{87}Rb/^{86}Sr$, and $^{87}Sr/^{86}Sr$ values, in most cases, yield the least altered samples. In a few samples, however, it appears that WR carbonate is slightly less altered than the NLM carbonate chosen for analysis. This observation further underscores the heterogeneity within individual samples. For these, only WR values are reported (Table 1).

5.3 Secular variations

5.3.1 Strontium

Strong and rapid secular variations in Sr isotopic compositions have been identified previously in Neoproterozoic successions [7,19,26], but our knowledge of the true magnitude and rate of Sr isotopic variations in the latest Neoproterozoic to Cambrian times has remained relatively poor.

The dashed line in Fig. 5 illustrates a previous estimate of the evolution of Sr isotopic compositions through Vendian time. In contrast, the solid band represents our current best estimate from data in Table 1 integrated from three separate Vendian basins. It is well known that $^{87}Sr/^{86}Sr$ in the ocean remains constant to within ~ 20 ppm, due to its long residence time of ~ 4 Ma. Thus, assuming our lowest $^{87}Sr/^{86}Sr$ values within each formation are representative of primary seawater values, we have constructed a thin band of possible secular variations in the Vendian ocean.

Prior to the Varanger glaciation, $^{87}Sr/^{86}Sr$ values in marine carbonates were relatively low (at present, values are known to range between 0.7065 and 0.7075) back to a major apparent hydrothermal event about 800 Ma ago [7,19]. Small fluctuations in $^{87}Sr/^{86}Sr$ of carbonate sam-

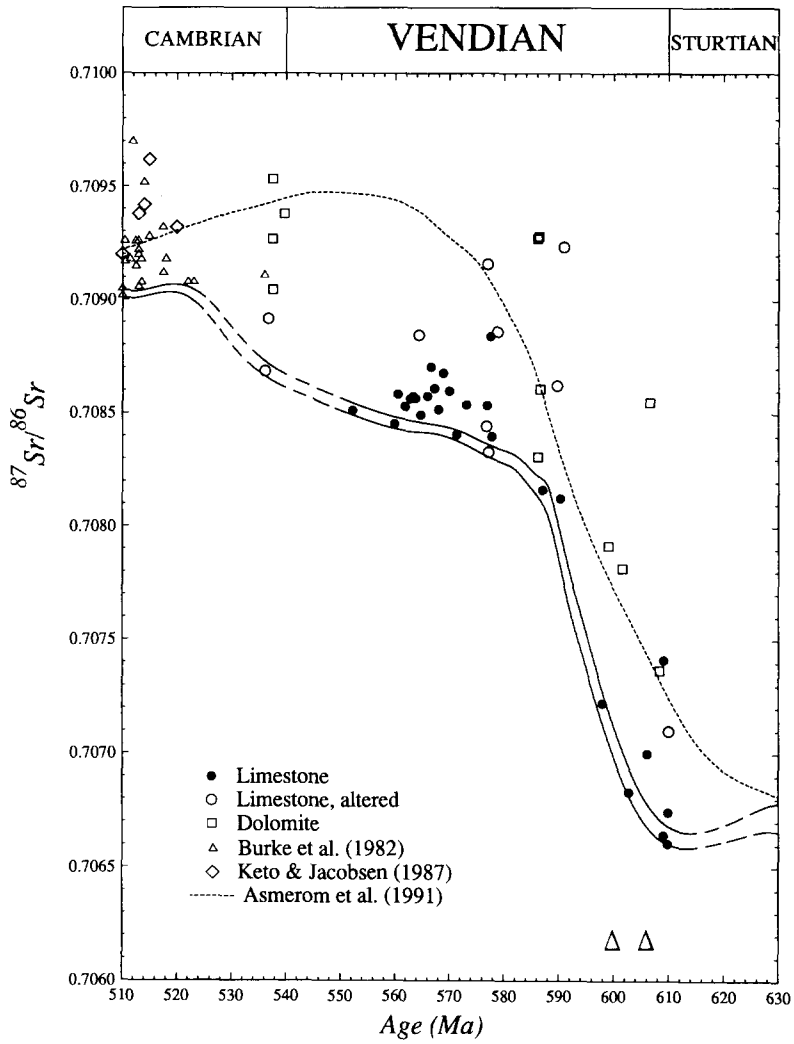

Fig. 5. Secular variation in $^{87}Sr/^{86}Sr$ of Vendian and Cambrian seawater estimated from well preserved limestones analyzed in this study. Middle and Late Cambrian data shown here are reported in [28,29]. Shaded symbols represent limestones and a single dolostone, which lie within the fields of least-altered samples shown in Fig. 4; outlined symbols represent limestones and dolostones which fall outside of these fields. Note that the dramatic rise in $^{87}Sr/^{86}Sr$ begins after the last glacial episode represented by the triangles plotted at 606 and 600 Ma. The average trend of Asmerom et al. [7] is shown as a dashed line.

ples deposited within the Varanger interval may result from enhanced erosion of platform sediments by glaciers during a sea-level draw-down; however, since $^{87}Sr/^{86}Sr$ values remain relatively low in a "cap" dolomite (actually a limestone in the sample under discussion) above the glacial horizon, this mechanism cannot account for the strong and rapid rise in Sr isotopic compositions in post-Varanger carbonates. Above the "cap" carbonates, Sr isotope values rise from 0.7071 to 0.7081 in the upper Witvlei Group (ca. 584 Ma) and plateau at values from 0.7084 to 0.7085 in the Schwarzrand Subgroup of the Nama Group (ca. 570–552 Ma). There is a large spread of $^{87}Sr/^{86}Sr$ values in the Nomtsas Formation, but the least-altered microsample suggests a value of 0.7087 for earliest Cambrian time. However, breaks in our curve for the Vendian (Fig. 5) emphasize that detailed patterns of secular change in $^{87}Sr/^{86}Sr$ across the Precambrian–Cambrian boundary cannot be determined from a single sample. Finally, data from Burke et al. [28], Keto and Jacobsen [29] and Donnelly et al. [30] suggest that in Middle and Late Cambrian times $^{87}Sr/^{86}Sr$ values rose to a maximum of 0.7091 and then fell to 0.7090 near the Cambrian–Ordovician boundary.

The least-altered dolostone samples show a strong secular trend in Sr isotopes similar to that obtained by the least-altered limestones, but values are offset towards substantially higher $^{87}Sr/^{86}Sr$ (Fig. 5). This may explain why $^{87}Sr/^{86}Sr$ values reported in a preliminary study of a dolomitic succession in Oman show substantially higher values than those reported here [31]. Although dolomitization removed Sr from pre-existing limestones, the process apparently did not completely obliterate the signal of strong secular $^{87}Sr/^{86}Sr$ variation during terminal Proterozoic

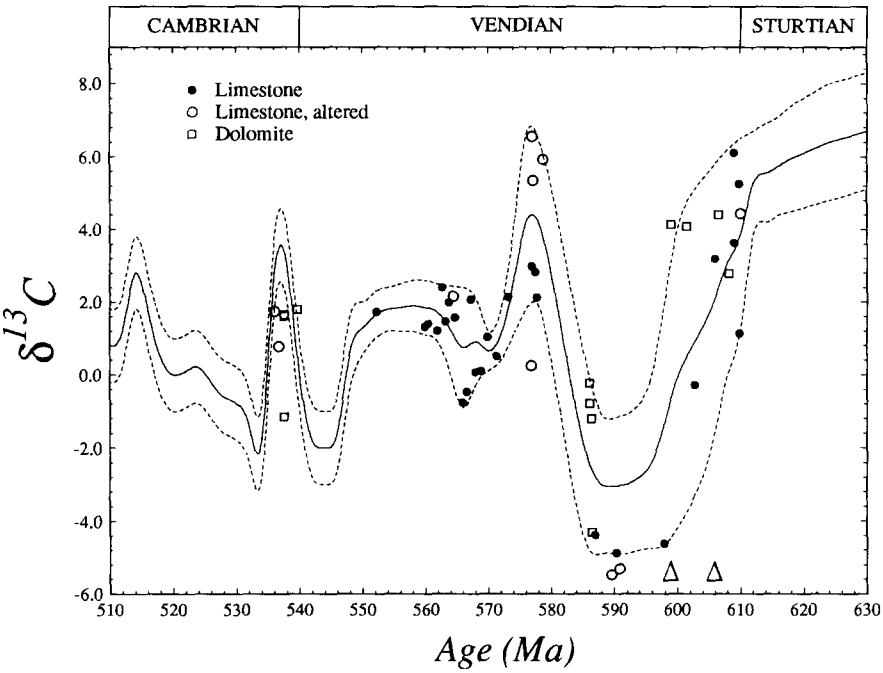

Fig. 6. Secular variations in $\delta^{13}C$ of Vendian and Cambrian seawater modified from fig. 4 of [8] with data from this study. Additional data for the interval between 535 to 560 Ma are from [33 and 22]. Middle and Late Cambrian data is compiled from Brasier [32]. Upper and lower limits of the secular curves represent uncertainty related to $\delta^{13}C$ variations within modern oceans, as well as possible variations in $\delta^{13}C$ related to facies.

time. From these results we conclude that, although Sr isotopic abundances in dolostones might be useful for correlation during times of rapid change, they usually do not record primary seawater Sr isotopic values.

5.3.2 Carbon

Fig. 6 shows the secular variation in C isotopes from Vendian to Cambrian time. This result is compiled from the present data base for the time interval 610–560 Ma, as well as numerous other C isotopic studies on Neoproterozoic and Cambrian successions [22,32,33] for the time 560–510 Ma. We note that dolostones appear to follow the same trend as limestones. With careful selection they can probably also be used to reconstruct trends in seawater $\delta^{13}C$ evolution. Prior to the Varanger Ice Age, $\delta^{13}C$ values of limestone and dolostone were typically high, averaging around +6, with some successions recording values as high as +8 to +10 or more. These highly positive $\delta^{13}C$ values are followed by a rapid excursion to negative $\delta^{13}C$ values of around −3 to −4, a likely response to enhanced ocean circulation and increased erosion of sedimentary organic C during and immediately following the Varanger glaciation. Carbon isotopic compositions remained negative until about 585 Ma and then increased rapidly to positive $\delta^{13}C$ values, peaking at +5 to +6 at about 575 Ma. Although the positive peak in $\delta^{13}C$ values is not represented by our highest quality samples, our confidence in its existence is enhanced by the fact that it occurs on five continents in every early Vendian sequence where isotopic studies have been conducted. The first fossil evidence of complex Ediacaran metazoans is found in rocks that document this increase in $\delta^{13}C$. Through the rest of the Vendian and into the Cambrian, $\delta^{13}C$ fluctuates between positive and negative values but the variations are generally smaller than those recorded in earlier Vendian time. The residence time of C (ca. 8×10^4 y) in the ocean is sufficiently short that inter- and intra-basinal variations should be expected. Natural variations recorded in the modern ocean confirm this, so we include approximate upper and lower bounds for the Vendian to Cambrian C isotope curve (Fig. 6).

6. Discussion

6.1 The Neoproterozoic record of Nd isotopic variations in seawater

The present Nd budget of the oceans is dominated by the river water (RW) flux (J_{Nd}^{RW}) from continental sources which vary in both their concentration and isotopic composition [34,35]. In contrast, the mid-ocean ridge hydrothermal water (HW) Nd flux today (J_{Nd}^{HW}) is only about 1% of the total Nd input to the oceans. Thus, variation of $^{143}Nd/^{144}Nd$ (expressed as ϵ_{Nd}) in seawater (SW) is primarily due to changes in the Nd isotopic composition of the continental flux to the oceans. The Nd isotopic mass balance is:

$$\tau_{Nd}\frac{d\epsilon_{Nd}^{SW}}{dt} = \frac{J_{Nd}^{HW}}{J_{Nd}^{RW}}\left(\epsilon_{Nd}^{HW} - \epsilon_{Nd}^{SW}\right) + \left(\epsilon_{Nd}^{RW} - \epsilon_{Nd}^{SW}\right) \quad (2)$$

where the left-hand side of eq. (2) is ≈ 0 because of the short residence time of Nd in seawater ($\tau_{Nd} \sim 10^3$ y). Furthermore, this short residence time is the principal reason for the large variations in ϵ_{Nd} recorded within both modern and ancient oceans. However, since the characteristic ϵ_{Nd} value of each ocean reflects that mixed from numerous source terrains, the average ϵ_{Nd} value of the oceans through time can be useful for tracing the isotopic evolution of the continental crust.

A global mean ϵ_{Nd} curve for the Phanerozoic has been constructed by averaging ϵ_{Nd} values of various paleo-oceans [36] and these results show that global seawater ϵ_{Nd} values were extremely low during the Cambrian (values range between −10 to −15). In contrast, due to: (1) uncertainty in the number and size of Neoproterozoic paleo-oceans; (2) the small number of chemical sediments analyzed; and (3) large uncertainty in the ages of samples; the record of Nd isotope variations in Neoproterozoic seawater is poorly constrained. Nonetheless, it appears from limited data on phosphorites and banded iron formations [36–38] that there is a significant decrease in seawater ϵ_{Nd} values from middle Neoproterozoic time, where values average around −4, to the

Cambrian average of −12. Because of the significant uncertainty in this secular trend and its considerable impact on models of sedimentary cycling [7,8] much additional work on the Nd isotopic composition of Neoproterozoic chemical sediments is needed.

6.2 Comparison of the Cenozoic and Vendian, Sr, C and Nd isotopic variations in seawater

A comparison of the Sr, Nd and C seawater isotope records for the Vendian–Cambrian and Cenozoic are shown in Fig. 7. Also shown are the

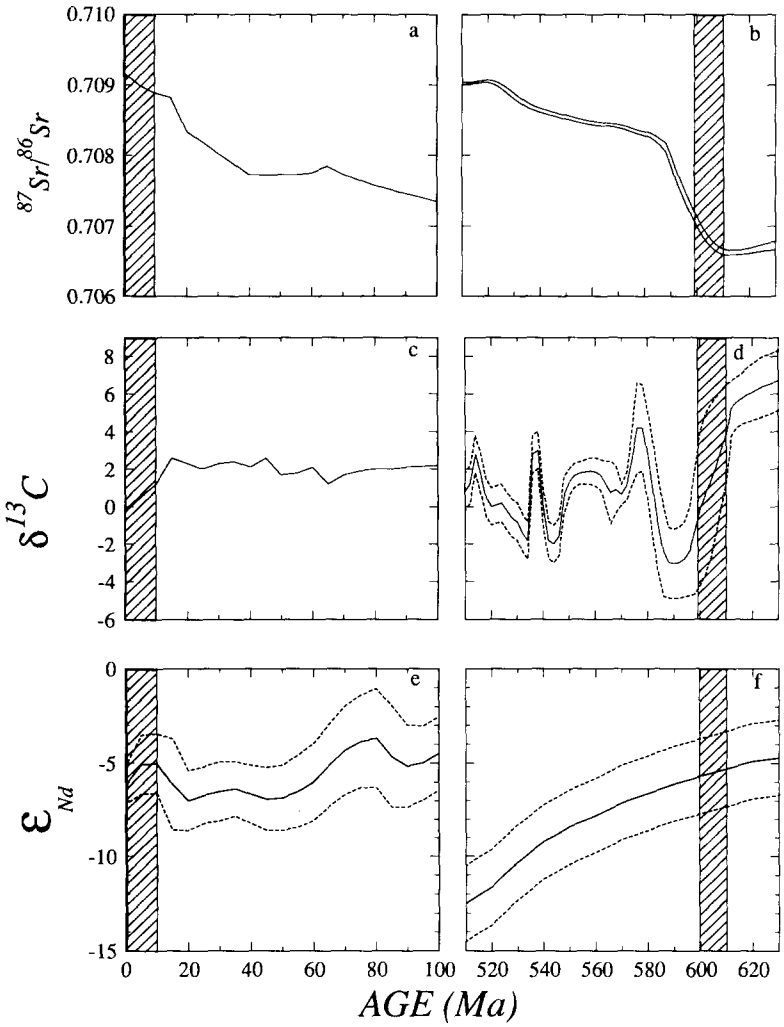

Fig. 7. Comparison of secular variations in the Sr-, C- and Nd-isotopic compositions of Cenozoic and Vendian–Cambrian seawater. Data for the Cenozoic variations in $^{87}Sr/^{86}Sr$ (Fig. 7a) from [1,3], in $\delta^{13}C$ (Fig. 7c) from [39] (the Cenozoic C isotope curve was constructed from analyses of deep sea carbonate), and in ϵ_{Nd} (Fig. 7e) from [29,38]. The uncertainty given for some of the curves relates to heterogeneities within the oceans, as well as uncertainties associated with the small number of analyses of Nd isotopes in sequences deposited during Neoproterozoic time. Shaded regions represent the major glacial intervals in the Cenozoic and Vendian Periods.

positions of the recent (0–10 Ma) and Varanger (598–610 Ma) glacial episodes. Rates of Sr isotopic increase were particularly high between 600 and 580 Ma ago (Fig. 7b), similar to those recorded between 40 and 15 Ma ago (Fig. 7a). Compared to the Cenozoic rise in $^{87}Sr/^{86}Sr$ of seawater, our current best estimate of the Sr isotope curve during the Vendian shows an even larger change. Nonetheless, the striking similarity in both trends suggests a similarity of orogenic events leading to an increase in the erosional flux of Sr from continental sources. The Vendian record of $^{87}Sr/^{86}Sr$ variations probably requires that Pan-African orogenesis produced Himalayan-scale mountains [7]. In strong contrast to the Cenozoic record, however, Neoproterozoic glaciations all precede the rise in Sr isotopic compositions. Note that Fig. 7 does not show the earlier Neoproterozoic ice ages, which occurred during a long interval characterized by relatively low $^{87}Sr/^{86}Sr$.

The strong secular variation noted in C isotopic abundances in Vendian to Cambrian successions (Fig. 7d) is not evident in the Cenozoic record [39] (Fig. 7c). As discussed above, enrichment in ^{13}C of Neoproterozoic platform carbonates has been attributed to stratification of ocean basins in which ^{13}C-depleted organic C could accumulate in sediments beneath anoxic deep water. However, the rapid excursion to negative ^{13}C values at Varanger time is attributed to the mixing of ^{13}C-depleted deep water with shallow water on carbonate platforms during glacially enhanced circulation of the world ocean [16] and, possibly, to increased erosion of organic C stored on shelves and platforms. A similar process may have led to the 2‰ depletion in ^{13}C abundances recorded in marine carbonates over the past 20 Ma of the Cenozoic. The magnitude of the effect is smaller, however, and there is no evidence for ocean stratification immediately prior to Cenozoic glaciation.

There is little variation in the averaged Nd isotopic composition of Cenozoic oceans [36], with only a suggestion of a slight rise in ϵ_{Nd} over the past 20 Ma (Fig. 7e). In comparison, Fig. 7f shows the long-term drop in ϵ_{Nd} in Vendian to Cambrian seawater described above. The constancy in late Cenozoic ϵ_{Nd} for the Indian Ocean [36] is inconsistent with the suggestion by Edmond [5] that the increase in $^{87}Sr/^{86}Sr$ is solely due to the unroofing of a highly radiogenic metamorphic core complex. If the Edmond [5] interpretation were correct, ϵ_{Nd} of seawater, especially in the Indian Ocean, should have decreased toward the very low values ($\epsilon_{Nd} = -16$) typical of the complex [40].

6.3 Constraints on crustal evolution, tectonics and global erosion rates from Sr and Nd isotopic variations

From the pattern of Nd model ages in sediments, the period between 1,500 and 600 Ma appears to be a time of aging of the crust with the addition of relatively little juvenile material [2]. Tectonic processes primarily resulted in a reworking of old crust during this period. For the same time interval there is a large overall increase in $^{87}Sr/^{86}Sr$ of seawater. This increase results from the aging of the upper crust exposed to erosion, as well as a decrease in the hydrothermal contribution to the Sr budget. Superimposed on this long-term increase in $^{87}Sr/^{86}Sr$ are rapid fluctuations that correlate with tectonic events in the Neoproterozoic [7]. This record provides an important tool for studying secular trends in global tectonic processes and crust–mantle evolution.

A detailed comparison of tectonic events with $^{87}Sr/^{86}Sr$ must await more precise dating of geological events, as well as better age calibration of the $^{87}Sr/^{86}Sr$ seawater curve. However, the main features now appear to be well established. They are: very low $^{87}Sr/^{86}Sr$ associated with a major rifting event ca. 800 Ma ago and the very significant Vendian rise in $^{87}Sr/^{86}Sr$. The geological record shows evidence for the existence and breakup of an early supercontinent (i.e., Rodinia), followed by the widespread Pan-African orogenic event in which the Gondwana supercontinent was assembled. This orogeny affected much of present day Africa, Europe and Asia [41–43].

Tectonically driven increases or decreases in continental erosion are assumed to have strong effects on the variation of $^{87}Sr/^{86}Sr$ in seawater. Secular change in $^{87}Sr/^{86}Sr$ is controlled both by

changes in the ratio of the river water flux (J_{Sr}^{RW}: the erosional flux) of Sr from the continents and the hydrothermal flux (J_{Sr}^{HW}) of Sr through ocean ridges (at least 10–20% of the total input today), as well as by changes in the isotopic composition of these fluxes. The mass balance equation for $^{87}Sr/^{86}Sr$ (expressed as ϵ_{Sr}) of seawater is:

$$\tau_{Sr}\left(\frac{d\epsilon_{Sr}^{SW}}{dt}\right) = \left(\frac{J_{Sr}^{HW}}{J_{Sr}^{RW}}\right)\left(\epsilon_{Sr}^{HW} - \epsilon_{Sr}^{SW}\right) + \left(\epsilon_{Sr}^{RW} - \epsilon_{Sr}^{SW}\right) \quad (3)$$

where τ_{Sr} (~ 4.1 Ma) is the residence time of Sr in the oceans. The ϵ_{Nd} and ϵ_{Sr} variations in present river waters roughly obey the following relationship: $\epsilon_{Sr}^{RW} \approx \alpha\epsilon_{Nd}^{RW} + \beta$ where α and β are constants [35]. Calculations based on *both* the Nd and Sr isotopic variations in seawater with time can be used to estimate changes in the relative importance of the river and the hydrothermal flux of Sr to the oceans through time [2,7] using:

$$\left(\frac{J_{Sr}^{RW}}{J_{Sr}^{HW}}\right) = \left[\frac{\left(\epsilon_{Sr}^{HW} - \epsilon_{Sr}^{SW}\right) - \alpha\gamma\left(\epsilon_{Nd}^{HW} - \epsilon_{Nd}^{SW}\right)}{\tau_{Sr}\left(\frac{d\epsilon_{Sr}^{SW}}{dt}\right) - \left(\alpha\epsilon_{Nd}^{SW} + \beta - \epsilon_{Sr}^{SW}\right)}\right] \quad (4)$$

where $\gamma = (Nd/Sr)_{HW}/(Nd/Sr)_{RW}$ [2,7]. Estimates of $\alpha = 6.44$, $\beta = 52$ and $\gamma = 0.09$ were obtained from [7,35] and are consistent with a present average $^{87}Sr/^{86}Sr = 0.711$ for the global river water flux [3,35,44,45]. Estimates of ϵ_{Nd} and ϵ_{Sr} in the hydrothermal component can be evaluated using the Sr and Nd isotopic evolution of the depleted mantle through time.

In so far as the global dissolved flux of Sr in rivers is proportional to the global erosion rate [2], the J_{Sr}^{RW} value constrained by eq. (4) *is a*

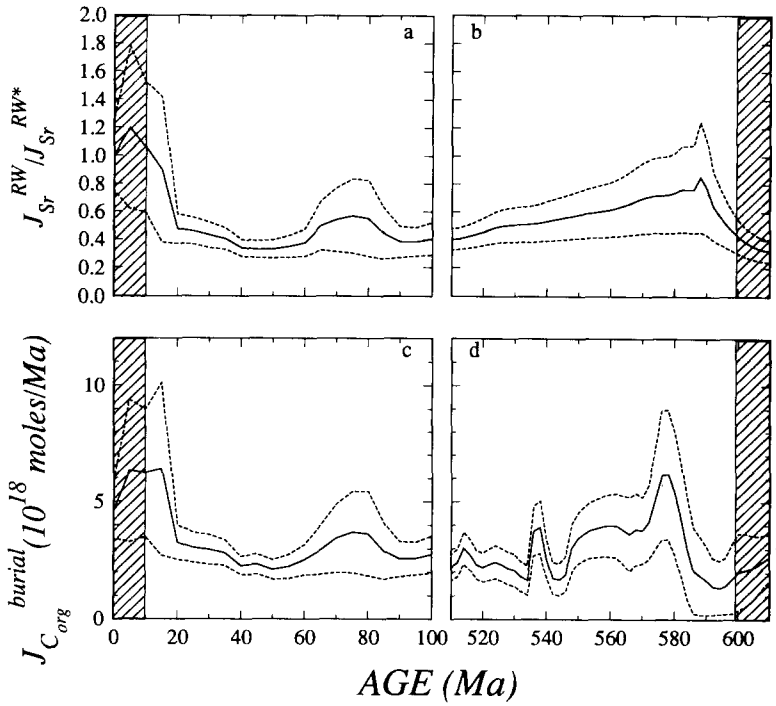

Fig. 8. Calculated variations in erosion rates (J_{Sr}^{RW}/J_{Sr}^{RW*}) and C burial rates (J_{Corg}^{burial}), using the model discussed in the text (eqs. 4 and 6). Shaded regions represent the major glacial intervals in the Cenozoic and Vendian Periods. Error bands shown are based on the uncertainties of the isotope curves shown in Fig. 7.

proxy of erosion rates through time. We note that this does not necessarily imply that $^{87}Sr/^{86}Sr$ in seawater is a proxy for erosion rates. Most likely the ϵ_{Sr}^{SW} value is a function of *both* varying erosion rates and changes in the $^{87}Sr/^{86}Sr$ of the river flux.

Two extreme views have been presented for the interpretation of the seawater $^{87}Sr/^{86}Sr$ curve: (1) $^{87}Sr/^{86}Sr$ principally reflects variations in erosional fluxes from the continents [4,9,46], and (2) $^{87}Sr/^{86}Sr$ principally reflects the varying isotopic compositions of continental rocks subject to erosion [5,47]. Jacobsen [2] developed a simple first-order model (using the isotopic records of Sr and Nd in marine samples) that may be used to distinguish between these two end-member hypotheses. His model results [see also 7] indicate three distinct episodes of high global flux ratio, J_{Sr}^{RW}/J_{Sr}^{HW}, over the past 700 Ma. This was attributed primarily to very high global continental erosion rates during uplift, caused by continental collisions at: ~0–30 Ma (Himalayan–Tibetan collision), ~400 Ma (Caledonian–Appalachian collision) and ~600 Ma (Pan-African collision) ago [2,7]. Two of these episodes occurred during an interval of very rapid increase in $^{87}Sr/^{86}Sr$ (~0–30 Ma and ~600 Ma), while the third event (~400 Ma) did not. Thus, it appears that there is only a limited correlation between the Sr isotope curve and high versus low erosional fluxes. This pattern also contradicts the idea that $^{87}Sr/^{86}Sr$ of seawater predominantly reflects variations in the isotopic composition of the erosional flux from continents [5]. Other evidence comes from a model of Richter et al. [3], who suggest that about 50% of the Cenozoic increase in $^{87}Sr/^{86}Sr$ since the Eocene is attributable to increased Sr flux and the other 50% is due to the increased $^{87}Sr/^{86}Sr$ of the dissolved Sr flux in rivers.

Processes operating during the Vendian and Cambrian periods resulted in the largest change observed in $^{87}Sr/^{86}Sr$ of seawater at any time during the Earth's history (Fig. 7). It is possible that the rapid rise is primarily due to changes in rock composition and/or mean age of eroding rocks. For example, Hoffman [43] has suggested that a supercontinent was turned inside out at about this time, resulting in the erosion of rifted margins of old cratons. This is one possible mechanism for a rapid change in $^{87}Sr/^{86}Sr$ of the erosional flux.

The Vendian–Cambrian Sr and Nd isotopic curves in Fig. 7 were used to calculate J_{Sr}^{RW} (using eq. 4) for the period 510–650 Ma. The resulting J_{Sr}^{RW} curve shows a peak at ~580–590 Ma (Fig. 8b) suggesting that the change is the result of enhanced erosion associated with Pan-African orogenesis. The significant decrease in ϵ_{Nd} of seawater through the Vendian suggests that the $^{87}Sr/^{86}Sr$ of the river water flux did increase somewhat at this time. However, in spite of this change, a very large increase in the J_{Sr}^{RW} is still necessary to account for the very large increase in $^{87}Sr/^{86}Sr$. In contrast, the Cenozoic J_{Sr}^{RW} curve (Fig. 8a) shows a peak at ~5 Ma which, given the constancy of oceanic Nd isotopic compositions through this interval (Fig. 7e), does not appear to be correlated with any significant change in the $^{87}Sr/^{86}Sr$ of the river water flux to the oceans.

6.4 Constraints on organic C burial and the evolution of O_2 in the atmosphere

The variation of $\delta^{13}C$ of seawater (and marine carbonates) over time scales of crustal recycling is controlled both by changes in the global organic C erosion rate ($J_{C_{org}}^{erosion}$) and by changes in the rate of C burial ($J_{C_{org}}^{burial}$). The rate of change of crustal organic C (C_{org}) is a balance between burial and erosion:

$$\frac{dC_{org}}{dt} = J_{C_{org}}^{burial} - J_{C_{org}}^{erosion} = J_{C_{org}}^{burial} - k_{C_{org}} C_{org} \quad (5)$$

where $k_{C_{org}}$ is the time parameter for erosion of organic C. This mass balance equation can be coupled with the Sr, Nd and C isotopic records of seawater to yield estimates of the organic C burial rate. To couple the Sr and C cycles it is assumed that the erosion rate for Sr is proportional to that of organic C (i.e., $k_{C_{org}} = k^*_{C_{org}}(J_{Sr}^{RW}/J_{Sr}^{RW*})$ where the asterisk denotes the present-day value.

Assuming that the rate of recycling of carbonate rocks and sedimentary organic C is equal, then, by using eq. (5) and the isotopic mass balance for C, the burial rate of organic C shows a

simple relationship to overall erosion rates and secular variations in $\delta^{13}C$ of seawater [8]:

$$J_{C_{org}}^{burial} = \frac{M_{tc}}{\Delta} k_{C_{org}}^{*} \left(\frac{J_{Sr}^{RW}}{J_{Sr}^{RW*}} \right) \left(\delta^{13}C_{carb} - \delta^{13}C_{tc} \right) \quad (6)$$

Here the $\delta^{13}C$ values of the carbonate ($\delta^{13}C_{carb}$) and organic ($\delta^{13}C_{org}$) C reservoirs are related by the average exogenic carbon isotope value of $\delta^{13}C_{tc} = -5.5$. Further, for the Neoproterozoic, $\delta = \delta^{13}C_{carb} - \delta^{13}C_{org}$ is considered to be reasonably constant at 28.5 [11]. Eqs. (4) and (6) provide the basis for obtaining changes in erosion (J_{Sr}^{RW}) and organic C burial rates (J_{Corg}^{burial}) as a function of time, based on the Sr, C and Nd isotopic records of seawater. The calculated rate of organic C burial depends on the product of the erosion rate and ($\delta^{13}C_{carb} - \delta^{13}C_{tc}$) values in carbonates. Thus, it is possible to have relatively low $\delta^{13}C$ values (+1 to +2) in marine carbonates during periods of high organic carbon burial, if the erosion rate is very high. The changes in J_{Sr}^{RW} and J_{Corg}^{burial} calculated using the isotope records shown in Fig. 7 and eqs. (4) and (6) are shown in Fig. 8 for both the Cenozoic and Vendian–Cambrian.

A new curve for the burial rate of organic C, constrained by the new C and Sr isotopic variations presented in this study, as well as a re-evaluation of secular variations in the Nd isotopic composition of Vendian seawater is shown in Fig. 8b. This curve shows a peak at ~575 Ma that is smaller than that of Derry et al. [8] because of the substantial improvements in the C and Sr isotopic records presented here for the Vendian.

The evolution of atmospheric O_2 is, in part, controlled by the rates that we can constrain from the above model results (J_{Corg}^{burial} and J_{Sr}^{RW}). The long-term accumulation of O_2 in the atmosphere is primarily due to inputs related to the reduction of C, Fe or S in the exogenic cycle and to burial of these in sediments. Atmospheric O_2 is consumed by oxidation of the same elements during erosion of crustal rocks, so the balance of these through time should, to a first approximation, indicate changes in pO_2. The erosion parameter for oxygen is k_{O_2} and, to a first approximation, the rate of change of O_2 in the atmosphere is:

$$\frac{dO_2^{atm}}{dt} = J_{O_2}^{in} - k_{O_2} O_2^{atm} \quad (7)$$

where $J_{O_2}^{in}$ is the input flux of O_2 to the atmosphere. For each mole of C buried in sediments, 1 mole of O_2 is released to the atmosphere. By ignoring the smaller effects from the Fe and S cycles, we may scale the second term on the right-hand side of eq. (7) to erosion rates determined from eq. (4) (i.e. $k_{O_2} = k_{O_2}^{*}(J_{Sr}^{RW}/J_{Sr}^{RW*})$ where the * again denotes present values) and the first term may be set equal to the burial rate of organic C determined from eq. (5). This yields the following equation:

$$\frac{dO_2^{atm}}{dt} = J_{C_{org}}^{burial} - \left(\frac{k_{O_2}^{*}}{J_{Sr}^{RW*}} \right) J_{Sr}^{RW} O_2^{atm} \quad (8)$$

which is a first approximation to linking the evolution of atmospheric O_2 to changes in the rates of sedimentary cycling.

Earlier model results suggest that in pre-Varanger time "O_2" liberated by organic C burial was largely consumed by reducing hydrothermal fluids and oxidation of sedimentary sulfide, thereby buffering any net changes in pO_2 [8]. Derry et al. [8] suggested that the Vendian peak in organic C burial, coupled with lower fluxes of reducing hydrothermal fluids, gave rise to a large increase in O_2 in the atmosphere after the Varanger glaciation. The somewhat smaller peak in organic C burial (shown in Fig. 8b) compared to that published in [8] is still sufficiently large enough to generate most of the O_2 in the present atmosphere (37.5×10^{18} mol).

Recent investigations into the secular variations of S isotopes in the Vendian [48] strongly suggest that the excess of O_2 was not balanced by concomitant oxidation of sedimentary sulfides. Model results for the Cenozoic record are shown in Fig. 8a. The apparent Cenozoic peak in J_{Corg}^{burial} perhaps represents the "Monterey Event" (~15–20 Ma). However, during the Phanerozoic such peaks in J_{Corg}^{burial} need not cause large changes in atmospheric O_2 levels, because they may be balanced by the S cycle [49, see also 8]. Other

likely problems with our simple model for the Cenozoic are that δ has been shown not to be constant [50], and we have assumed (perhaps incorrectly) that the $\delta^{13}C$ composition of deep sea carbonates represents the C isotopic composition of the bulk carbonate flux [39].

6.5 Relationship to atmospheric CO_2 and paleoclimate

The evolution of the atmospheric CO_2 is, in part, controlled by the erosion rate that we can constrain from the Sr and Nd records (J_{Sr}^{RW}). The long-term rate of change of atmospheric CO_2 is a balance between the input from the Earth's interior relative to the effect of erosion which consumes CO_2. To a first approximation we have:

$$\frac{dCO_2^{atm}}{dt} = J_{CO_2}^{in} - k_{CO_2}CO_2^{atm} \quad (9)$$

where $J_{CO_2}^{in}$ is the CO_2 input flux to the atmosphere. Here, k_{CO_2} is the erosion parameter for CO_2. However, as discussed by DePaolo [51] eq. 9 may have to be replaced with a non-linear equation for large changes in CO_2. The flux from the interior of the Earth is primarily due to the release of mantle CO_2 along mid-ocean ridges ($J_{CO_2}^{MORB}$ is the present mantle flux of CO_2 through mid-ocean ridge basalts) and it may be scaled to the hydrothermal flux of Sr ($J_{CO_2}^{in} = J_{CO_2}^{MORB}(J_{Sr}^{HW}/J_{Sr}^{HW*})$). The CO_2 consumption rate may be scaled to the erosion rate determined from the river water Sr flux and we obtain:

$$\frac{dCO_2^{atm}}{dt} = \left(\frac{J_{CO_2}^{MORB}}{J_{Sr}^{HW}}\right) J_{Sr}^{HW} - \left(\frac{k_{CO_2}^{*}}{J_{Sr}^{RW*}}\right) J_{Sr}^{RW} CO_2^{atm} \quad (10)$$

This equation provides a first approximation of the quantitative linkage between atmospheric CO_2 and tectonics in the way proposed by Chamberlin [52]. He proposed that tectonics and climate are linked by atmospheric pCO_2. Increased rates of chemical weathering and erosion associated with orogenic uplift diminish pCO_2, resulting in global cooling. Eqs. (4) and (10) form a simple system in which the Sr and Nd-isotopic records allow evaluation of erosion rates, as well as the evolution of CO_2 in the atmosphere and its relation to climate changes.

For the Cenozoic it is suggested, by using $\epsilon_p = \delta^{13}C_{carb} - \delta^{13}C_{porphyrins}$ as a proxy for pCO_2 [53], that atmospheric pCO_2 has decreased by about a factor of 3 since the Cretaceous. Assuming a uniform change in pCO_2, use of eq. (10) suggests that the decrease in pCO_2 is consistent with a threefold increase in weathering rates over the same period, assuming no change in other terms of this equation. This is consistent with the increased weathering rate obtained from the Sr and Nd records in Fig. 8a, as well as of Jacobsen [2]. Raymo et al. [4] argued that Neogene continental glaciation can be related to uplift and erosion of the Himalayas, Andes and Tibetan Plateau over the last 30 Ma and that these tectonic events resulted in: (1) a lowering of atmospheric CO_2; and (2) a change in atmospheric circulation; which together resulted in the climatic changes evident in the recent glacial epoch.

The Neoproterozoic Era was a time of repeated continental glaciation, including one of the Earth's most severe refrigerations, the Varanger Ice Age of ~ 610–590 Ma ago [54]. It is of particular interest to correlate the changes in $^{87}Sr/^{86}Sr$ of seawater and the calculated value of J_{Sr}^{RW} with the timing of these latest Proterozoic glaciogenic rocks. If increased weathering leads to reduction of CO_2 and glaciation, then glaciations should occur at times of high $^{87}Sr/^{86}$ Sr, if this parameter is a proxy of erosion as assumed by Raymo [9]. However, if J_{Sr}^{RW} is used as a proxy for weathering, as suggested by Jacobsen [2], then glaciation should correlate with highs in this parameter. Figs. 7 and 8 show that for the Neoproterozoic neither is the case. The Varanger Ice Age occurs at the very beginning of the terminal Proterozoic rise in $^{87}Sr/^{86}Sr$ of seawater and not at the maximum, as today. The peak in J_{Sr}^{RW} also postdates the Varanger glaciation. Indeed, the high $^{87}Sr/^{86}Sr$ ratios but low J_{Sr}^{RW} of Cambrian rocks are associated in time with what is generally regarded as one of the warmest intervals of the Paleozoic Era. Similarly, the Sturtian Ice Age of ca. 735–725 Ma ago [55] does not come close to a peak in either $^{87}Sr/^{86}Sr$ or J_{Sr}^{RW}. Instead, it occurs during a long period of low and uniform

J_{Sr}^{RW} and $^{87}Sr/^{86}Sr$ in seawater [7]. We note that, in the Cenozoic, Antarctic ice sheets first formed ca. 35 Ma ago, near the beginning of the principal rise in $^{87}Sr/^{86}Sr$. While this provides an apparent parallel to the Varanger relationship, Cenozoic ice sheets expanded as $^{87}Sr/^{86}Sr$ rose, while Neoproterozoic ice sheets disappeared. Thus, a detailed comparison of the Cenozoic and Vendian suggest a more complex relationship between climate, continental erosion rates, glaciation and changes in atmospheric pCO_2 than previously envisioned.

In conclusion, ice ages mark both the Neoproterozoic and Cenozoic, but different stratigraphic relationships between Sr isotopic increase and continental glaciation indicate that uplift-driven models proposed to explain Cenozoic climatic change cannot account for latest Proterozoic ice ages. In so far as the Neoproterozoic Sr and Nd isotopic curves appear to rule out high erosion rates prior to and during glacial periods, one must look to factors such as high rates of organic C burial in an episodically stratified Neoproterozoic ocean to explain decreases in pCO_2 that could facilitate the growth of continental ice sheets. It is likely that atmospheric pCO_2 levels have exerted a primary control on global climate through geological time, but the potential controls on pCO_2 are variable. While continental "weatherability" and CO_2 emission associated with seafloor spreading certainly contribute to pCO_2, changes in the position of the lysocline, rates of organic C burial, seafloor weathering and other factors may also be important. Global climate changes also depend on other factors; such as the position and profile of continents, sea level, ocean and atmospheric circulation.

Acknowledgements

This work was funded by NSF grant EAR-9118628 to SBJ and NSF grant BSR90-17747 to AHK. We wish to thank Pieter Gresse and Wulf Hegenberger, as well as the geological surveys of South Africa and Namibia, for field support. Additional samples for this study were generously provided by Ian Fairchild, Keene Swett and Guy Narbonne. Discussions with Gerard Germs and Charlie Hoffmann also helped resolve stratigraphic problems between units in South Africa and Namibia. Finally, we wish to thank Louis Derry, Jan Veizer and Donald DePaolo for constructive reviews, and Ronald Pflaum, as well as numerous Harvard undergraduate students who helped in sample preparation and analysis.

References

[1] D.J. DePaolo and B.L. Ingram, High-resolution stratigraphy with strontium isotopes, Science 227, 928–941, 1985.
[2] S.B. Jacobsen, Isotopic constraints on crustal growth and recycling, Earth Planet. Sci. Lett. 90, 315–329, 1988.
[3] F.M. Richter, D.B. Rowley and D.J. DePaolo, Sr isotope evolution of seawater: The role of tectonics, Earth Planet. Sci. Lett. 109, 11–23, 1992.
[4] M.E. Raymo, W.F. Ruddiman and P.N. Froelich, Influence of late Cenozoic mountain building on ocean geochemical cycles, Geology 16, 649–653, 1988.
[5] J.M. Edmond, Himalayan tectonics, weathering processes, and the strontium isotope record in marine limestones, Science 258, 1594–1597, 1992.
[6] A.H. Knoll and M.R. Walter, Latest Proterozoic stratigraphy and Earth history, Nature 356, 673–677, 1992.
[7] Y. Asmerom, S.B. Jacobsen, N.J. Butterfield and A.H. Knoll, Sr isotope variations in Late Proterozoic seawater: Implications for crustal evolution, Geochim. Cosmochim. Acta 55, 2883–2894, 1991.
[8] L.A. Derry, A.J. Kaufman and S.B Jacobsen, Sedimentary cycling and environmental change in the Late Proterozoic: Evidence from stable and radiogenic isotopes, Geochim. Cosmochim. Acta 56, 1317–1329, 1992.
[9] M.E. Raymo, Geochemical evidence supporting T.C. Chamberlin's theory of glaciation, Geology 19, 344–347, 1992.
[10] I.J. Fairchild and M.J. Hambrey, The Vendian succession of northeastern Spitsbergen: Petrogenesis of a dolomite–tillite association, Precambrian Res. 26, 111–167, 1984.
[11] A.H. Knoll, J.M. Hayes, A.J. Kaufman, K. Swett and I.B. Lambert, Secular variations in carbon isotope ratios from Upper Proterozoic successions of Svalbard and East Greenland, Nature 321, 832–838, 1986.
[12] I.J. Fairchild and P.M. Herrington, A tempestite–stromatolite–evaporite association (Late Vendian, East Greenland): A shoreface–lagoon model, Precambrian Res. 43, 101–127, 1989.
[13] G.J.B. Germs, Implications of a sedimentary facies and depositional environmental analysis of the Nama Group in South West Africa/Namibia, Spec. Publ. Geol. Surv. S. Afr. 11, 89–114, 1983.

[14] G.J.B. Germs and P.G. Gresse, The foreland basin of the Damara and Gariep orogens in Namaqualand and southern Namibia: Stratigraphic correlations and basin dynamics, S. Afr. J. Geol. 94, 159–169, 1991.
[15] K.H. Hoffmann, New aspects of lithostratigraphic subdivision and correlation of late Proterozoic to early Cambrian rocks of the southern Damara Belt and their correlation with the central and northern Damara Belt and Gariep Belt, Commun. Geol. Surv. Namibia 5, 59–67, 1989.
[16] A.J. Kaufman, J.M. Hayes, A.H. Knoll, and G.J.B. Germs, Isotopic compositions of carbonates and organic carbon from upper Proterozoic successions in Namibia: Stratigraphic variation and the effects of diagenesis and metamorphism, Precambrian Res. 49, 301–327, 1991.
[17] A. Kröner, The correlation of the pre-Cape sediments in the Vanrhynsdorp region, Cape Province, Trans. Geol. Soc. S. Afr. 72, 127–150, 1969.
[18] M. Schidlowski, R. Eichmann and C. Junge, Precambrian sedimentary carbonates: Carbon and oxygen isotopic geochemistry and implications for the terrestrial oxygen budget, Precambrian Res. 2, 1–69, 1975.
[19] J. Veizer, W. Compston, N. Clauer and M. Schidlowski, $^{87}Sr/^{86}Sr$ in Late Proterozoic carbonates: Evidence for a "mantle event" at 900 Ma ago, Geochim. Cosmochim. Acta 47, 295–302, 1983.
[20] J.D. Aitken, Uppermost Proterozoic formations in central Mackenzie Mountains, Northwest Territories, Geol. Surv. Can. Bull. 368, 1–26, 1989.
[21] J.D. Aitken, Two late Proterozoic glaciations, Mackenzie Mountains, northwestern Canada, Geology 19, 445–448, 1991.
[22] G.M. Narbonne, A.J. Kaufman and A.H. Knoll, Integrated chemostratigraphy and biostratigraphy of the Upper Windermere Supergroup, Mackenzie Mountains, Northwestern Canada, Geol. Soc. Am. Bull., in review, 1993.
[23] G.M. Narbonne and J.D. Aitken, Ediacaran fossils from the Sekwi Brook area, Mackenzie Mountains, Northwestern Canada, Paleontology 33, 945–980, 1990.
[24] N.H. Sleep, Thermal effects of the formation of Atlantic continental margins by continental break-up, Geophys. J.R. Astron. Soc. 4, 325–350, 1971.
[25] G.M. Narbonne, New Ediacaran fossils from the Mackenzie Mountains, northwestern Canada, J. Paleontol., in press, 1993.
[26] L.A. Derry, L.S. Keto, S.B. Jacobsen, A.H. Knoll and K. Swett, Sr isotopic variations in Upper Proterozoic carbonates from Svalbard and East Greenland, Geochim. Cosmochim. Acta 53, 2331–2339, 1989.
[27] K.W. Wedeking, J.M. Hayes and U. Matzigkeit, Procedures of organic geochemical analysis, in: Earth's Earliest Biosphere: Its Origin and Evolution, J.W. Schopf, ed., pp. 428–440, Princeton Univ. Press, Princeton, N.J., 1983.
[28] W.M. Burke, R.E. Denison, E.A. Hetherington, R.B. Koepnick, M.F. Nelson and J.B. Omo, Variations of seawater $^{87}Sr/^{86}Sr$ throughout Phanerozoic time, Geology 10, 516–519, 1982.
[29] L.S. Keto and S.B. Jacobsen, Nd and Sr isotopic variations of Early Paleozoic oceans, Earth Planet. Sci. Lett. 84, 27–41, 1987.
[30] T.H. Donnelly, J.H. Shergold, P.N. Southgate and C.J. Barnes, Events leading to global phosphogenesis around the Proterozoic/Cambrian boundary, in: Phosphorite Research and Development, A.J.G. Nothold and I. Jarvis, eds., Geol. Soc. London Spec. Publ. 52, 273–287, 1990.
[31] S.J. Burns and A. Matter, The strontium isotopic composition of Late Precambrian carbonates (~ 640–560 Ma) from Oman, Geol. Soc. Am. Abstr. Prog. 23, A97, 1991.
[32] M.D. Brasier, Towards a carbon isotope stratigraphy of the Cambrian System: potential of the Great Basin succession, in: High Resolution Stratigraphy, E.A. Hailwood and R.B. Kidd, eds., Geol. Soc. London Spec. Publ. 70, 341–350, 1992.
[33] M. Magaritz, W.T. Holser and J.L. Kirschvink, Carbon-isotope events across the Precambrian/Cambrian boundary on the Siberian Platform, Nature 320, 258–259, 1986.
[34] D.J. Piepgras, G.J. Wasserburg and E.J. Dasch, The isotopic composition of neodymium in different ocean masses, Earth Planet. Sci. Lett. 45, 223–236, 1979.
[35] S.J. Goldstein and S.B. Jacobsen, Nd and Sr isotopic systematics of river dissolved material: Implications for the sources of Nd and Sr in seawater, Chem. Geol. Isotope Geosci. Sect. 66, 245–272, 1987.
[36] L.S. Keto and S.B. Jacobsen, Nd isotopic variations of Phanerozoic Paleoceans, Earth Planet. Sci. Lett. 90, 395–410, 1988.
[37] H.F. Shaw and G.J. Wasserburg, Sm–Nd in marine carbonates and phosphates: Implications for Nd isotopes in seawater and crustal ages, Geochim. Cosmochim. Acta 49, 503–518, 1985.
[38] S.B. Jacobsen and M.R. Pimentel-Klose, Nd isotopic variations in Precambrian banded iron formations, Geophys. Res. Lett. 15, 393–396, 1988.
[39] N.J. Shackleton, Oceanic carbon isotope constraints on oxygen and carbon dioxide in the Cenozoic atmosphere, in: The Carbon Cycle and Atmospheric CO_2: Natural Variations Archean to Present, E.T. Sundquist and W.S. Broecker, eds., Am. Geophys. Union Geophys. Monogr. 32, 412–417, 1985.
[40] C. France-Lanord, L. Derry and A. Michard, Evolution of the Himalaya since Miocene time: Isotopic and sedimentary evidence from the Bengal Fan, in: Himalayan Tectonics, P.J. Treloar and M. Searle eds., Geol. Soc. London Spec. Publ., in press, 1993.
[41] G.C. Bond, P.A. Nickeson and M.A. Kominz, Breakup of a supercontinent between 625 Ma and 555 Ma: New evidence and implications for continental histories, Earth Planet. Sci. Lett. 70, 325–345, 1984.
[42] H. Porada, Pan-African rifting and orogenesis in southern to equatorial Africa and eastern Brazil, Precambrian Res. 44, 103–136, 1989.

[43] P.F. Hoffman, Did the breakout of Laurentia turn Gondwanaland inside-out?, Science 252, 1409–1412, 1991.
[44] M.R. Palmer and J.M. Edmond, The strontium isotope budget of the modern ocean, Earth Planet. Sci. Lett. 92, 11–26, 1989.
[45] S. Krishnaswami, J.R. Trivedi, M.M. Sarin, R. Ramesh and K.K. Sharma, Strontium isotopes and rubidium in the Ganga–Brahmaputra river system: Weathing in the Himalaya, fluxes to the Bay of Bengal and contributions to the evolution of oceanic 87Sr/86Sr, Earth Planet. Sci. Lett. 109, 243–253, 1992.
[46] L.M. Francois and J.C.G. Walker, Modeling the Phanerozoic carbon dioxide cycle and climate: constraints from the $^{87}Sr/^{86}Sr$ isotopic ratio of seawater, Am. J. Sci. 292, 81–135, 1992.
[47] R.A. Berner and D.M Rye, Calculation of the Phanerozoic strontium isotope record of the oceans from a carbon cycle model, Am. J. Sci. 292, 136–148, 1992.
[48] G.M. Ross, J.D. Bloch and H.R. Krouse, Sulphur isotope geochemistry of authigenic pyrite, late Proterozoic Windermere Supergroup, Cariboo Mountains, British Columbia, Geol. Assoc. Can. Abstr. Prog. 16, 108, 1991.
[49] J. Veizer, W.T. Holser and C.K. Wilgus, Correlation of $^{13}C/^{12}C$ and $^{34}S/^{32}S$ secular variations, Geochim. Cosmochim. Acta 44, 579–587, 1980.
[50] B.N. Popp, R. Takigiku, J.M. Hayes, J.W. Louda and E.W. Baker, The post-Paleozoic chronology and mechanism of ^{13}C depletion in primary marine organic matter, Am. J. Sci. 289, 436–454, 1989.
[51] D.J. DePaolo, Sr isotopes, atmospheric CO_2 and long-term climate change, EOS Trans. Am. Geophys. Union 72, 152, 1991.
[52] T.C. Chamberlin, An attempt to frame a working hypothesis of the cause of glacial periods on an atmospheric basis, J. Geol. 7, 545–584, 667–685, 751–787, 1899.
[53] K.H. Freeman and J.M. Hayes, Fractionation of carbon isotopes by phytoplankton and estimates of ancient CO_2 levels, Global Biogeochem. Cycles 6, 185–198, 1992.
[54] M.J. Hambrey and W.B. Harland, The Late Proterozoic glacial era, Palaeogeogr. Palaeoclimatol. Palaeoecol. 51, 255–272, 1985.
[55] C. Klein and N.J. Beukes, Sedimentology and geochemistry of glaciogenic Late Proterozoic Rapitan iron-formation in Canada, Econ. Geol. 88, 542–565, 1993.